Microchimica Acta (2020) 187:212
https://doi.org/10.1007/s00604-020-4209-8

ORIGINAL PAPER

Calcium ion assisted fluorescence determination of microRNA-167 using carbon dots–labeled probe DNA and polydopamine-coated Fe_3O_4 nanoparticles

Xiaodong Cao[1] · Kairui Zhang[1] · Wuwen Yan[1] · Zihao Xia[1] · Shudong He[1] · Xuan Xu[2] · Yongkang Ye[1] · Zhaojun Wei[1] · Songqin Liu[3]

Received: 4 November 2019 / Accepted: 2 March 2020

Abstract

A selective and sensitive fluorescence biosensor is described for determination of microRNA-167 using fluorescent resonant energy transfer (FRET) strategy. The FRET system comprises carbon dots (CDs, donor) labeled with probe DNA (pDNA) and polydopamine (PDA)-coated Fe_3O_4 nanoparticles (Fe_3O_4@PDA NPs, acceptor). The CDs-pDNA can be absorbed onto the surface of Fe_3O_4@PDA NPs because of the strong π interaction between pDNA and PDA. With the enhanced adsorption ability of Fe_3O_4@PDA NPs by Ca^{2+}, the fluorescence intensity of CDs at 445 nm (excitation at 360 nm) is quenched. In presence of microRNA-167, the hybridized complex of CDs-pDNA-microRNA-167 will be released from the surface of Fe_3O_4@PDA NPs due to the weak π interaction of the complex and PDA. This results in the fluorescence recovery of CDs. By application of twice-magnetic separation, the biosensor shows a wide linear range of 0.5–100 nM to microRNA-167 with a 76 pM detection limit. The method was applied to the determination of microRNA-167 in samples of total microRNA extractions from *A. thaliana* seedlings, and the recoveries ranged from 96.4 to 98.3%.

Keywords Fluorescence biosensor · Fluorescent resonant energy transfer · π interaction · Twice-magnetic separation · Hybridized complex · MicroRNA extractions

Introduction

MicroRNAs in plants have been becoming crucial regulation factors involving in phytohormone response pathways by affecting phytohormones' metabolism, distribution, and perception [1]. They not only regulate the responses to internal cues but also function in tolerance and responses to environmental/extrinsic stresses [2, 3]. MicroRNA-167 is one of few important conserved microRNAs that regulates auxin (indole-3-acetic acid, IAA) signaling through its targets [1, 2]. These target genes are positive regulators of root growth. The expression level of microRNA-167 may be altered under various circumstances during plant growth [4, 5]. For example, the exogenous supply of IAA can upregulate the expression level of microRNA-167 in root and shoots in *Brassica juncea* under arsenic stress. The function of microRNA-167 was augmented for the regulation of its target genes and growth of root [5]. Therefore, sensitive and selective methods for determination/monitoring the expression level change of a certain microRNA in plants are necessary to reveal the roles of microRNAs in plant growth under various circumstances.

The traditional detection methods for microRNAs are northern blotting [6], real-time quantitative polymerase chain reaction (RT-qPCR) [7], and microarray assays [8]. Apart from these conventional methods, various methods including

Electronic supplementary material The online version of this article (https://doi.org/10.1007/s00604-020-4209-8) contains supplementary material, which is available to authorized users.

✉ Yongkang Ye
yongkang.ye@hfut.edu.cn

✉ Songqin Liu
liusq@seu.edu.cn

[1] School of Food Science and Engineering, Hefei University of Technology, Hefei 230009, China

[2] School of Chemistry and Molecular Engineering, Nanjing Tech University, Nanjing 211816, China

[3] Jiangsu Province Hi-Tech Key Laboratory for Bio-medical Research, School of Chemistry and Chemical Engineering, Southeast University, Nanjing 211189, China

Published online: 10 March 2020

electrochemical and optical methods [9, 10] that based on biosensing have been largely developed for rapid, sensitive, and selective detection of microRNAs. These alternative methods show advantages of ease sample preparation, time saving, cost effectiveness, and portability. Therefore, the fabrication and application of electrochemical [11] and optical [12] biosensors for microRNAs have been widely investigated in the fields from clinical diagnostics and treatment to biological science.

Fluorescence-based biosensor is one of the commonly used optical biosensor for determination of microRNAs. There are two kinds of fluorescence biosensors, i.e., signal-on (fluorescence generation) and signal-off (fluorescence quenching) biosensors. They can achieve the detection of microRNAs by recording the signals after the hybridization event happened between target microRNAs and their complementary nucleic acids [9]. The fluorescence-based biosensor can gain high sensitivity and robustness by lowering background signal [13] and amplifying fluorescence intensity [14, 15]. In terms of reducing the background signal in fluorescence-based biosensors, the utilization of nanomaterials is a good choice to make it. These nanomaterials include graphene oxide (GO) [16], carbon nanotubes (CNTs) [17], gold nanoparticles (AuNPs) [18], transition metal disulfide nanosheets [19, 20], and polymer or polymer-coated nanomaterials [13, 21, 22]. Polydopamine (PDA) nanoparticles, a polymeric nanomaterial polymerized from dopamine (DA), have been recognized as an efficient fluorescence quencher in signal-off-based biosensing. This is mainly because of its outstanding biocompatibility and strong absorption ability towards single-strand DNA (ssDNA) by π stacking interaction [13, 21]. Xu et al. first reported spherical PDA nanospheres (336.0 ± 37.5 nm) showed strong fluorescence quenching ability with up to 97% quenching efficiency towards four kinds of fluorophores [21]. The synthesized PDA nanospheres were then used to construct biosensors based on fluorescent resonant energy transfer (FRET) strategy for determination of target DNA and thrombin. The detection limits of target DNA and thrombin were 0.1 and 0.5 nM, respectively. These results were close to those signal-off biosensors using GO-based nanomaterials as quenchers. An interesting and valuable finding has been discovered by Liu's group. They found that ssDNA strongly adsorbed on the surface of PDA nanospheres (~ 160 nm) via polyvalent Ca^{2+}-mediated coordination [22]. Such adsorption showed excellent resistance to DNA displacement by different biological ligands. They concluded that the resistance enabled the sensing platform to possess the advantage in practical application in real biological samples without great interference from the sample matrix. Another way to improve the sensitivity of fluorescence biosensors was to select fluorescent probes with high intensity and stability combining with signal amplification strategy. Various kinds of fluorescent nanostructured reporters like graphene quantum dots (GQDs) [23], carbon dots (CDs) [24], some other inorganic quantum dots [25], and metal nanoclusters [26, 27] are synthesized and used in constructing fluorescence biosensors. For instance, Hamd-Ghadareh et al. [24] described a ratiometric fluorescence biosensor for microRNA-155. The sensing platform was based on FRET using fluorescent dye–conjugated CDs probe and AuNPs as the energy donor-acceptor and rhodamine B (RB) as signal amplification reagent. The biosensor shows excellent sensitivity that it can work at attomolar concentration level of microRNA-155. They claimed that superb selectivity was resulted from broad emissions of CDs and internal reference of RB. Luo et al. [26] used PDA nanosphere as fluorescence quencher to accept the fluorescence from gold nanoclusters. By using DNase-I-assisted target recycling amplification strategy, the sensing platform can realize sensitive detection of microRNA-21 and let-7a with detection limits of 4.2 and 3.6 pM, respectively.

Iron oxide (Fe_3O_4) nanoparticles have been widely used in biosensing owing to the superparamagnetism, good biocompatibility, and ease of preparation and functionalization [28]. Herein, we presented a sensitive and selective fluorescence biosensor for determination of microRNA-167. The detection strategy is based on FRET using CDs as a fluorescence donor and Fe_3O_4@PDA NPs as a fluorescence acceptor. The sensitive determination for microRNA-167 is achieved by taking advantages of magnetic separation of Fe_3O_4, marvelous fluorescence quenching ability of PDA, and enhanced absorption capability of PDA to ssDNA with assistance of Ca^{2+}. Scheme 1 displays the fluorescence tags' fabrication and detection procedures of the biosensor. Here, carboxy-rich CDs with high fluorescence intensity and good stability were synthesized and then biofunctionalized with pDNA via covalent bonding. In presence of Ca^{2+}, the binding pDNA was strongly adsorbed on Fe_3O_4@PDA NPs through Ca^{2+} coordination and π stacking between the nucleobases and PDA. The fluorescence of modified CDs can be quenched significantly due to FRET from CDs to Fe_3O_4@PDA NPs. In presence target microRNA-167, pDNA absorbed on the surface of Fe_3O_4@PDA NPs can hybridize with microRNA due to target recognition. Owing to the weak interaction between the hybridized complex and Fe_3O_4@PDA NPs [21, 29], the CDs-labeled pDNA and microRNA hybrids were then liberated from the surface of Fe_3O_4@PDA NPs. This leads to the fluorescence recovery of CDs. The biosensing of microRNA-167 without signal amplification steps was fast and simple. The method can be used for direct determination of microRNA-167 in total microRNA extractions from *A. thaliana* seedlings.

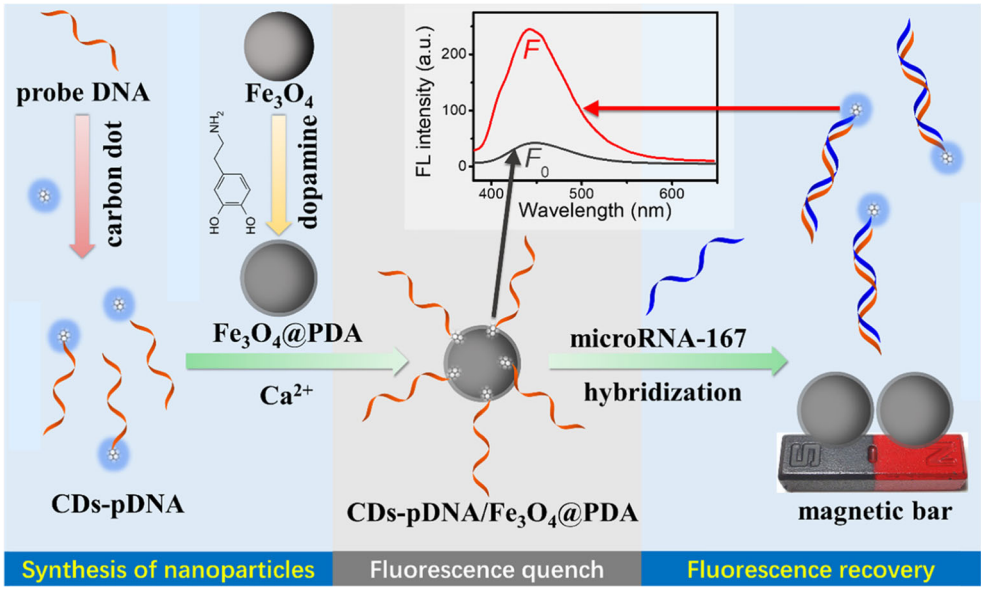

Scheme 1 Schematic representation of the fabrication of fluorescence tags and detection procedures of the biosensor

Experimental

Materials and reagents

Citric acid (CA), ethylenediamine (EDA), and calcium chloride anhydrous ($CaCl_2$) were purchased from National Medicine Group Shanghai Chemical Reagent Co., Ltd. (Shanghai, China). N-(3-Dimethylaminopropyl)-N′-ethylcarbodiimide hydrochloride (EDC), N-hydroxysuccinimide (NHS), Fe_3O_4 NPs, and dopamine hydrochloride (DA) were bought from Aladdin (Aladdin Industrial Co. Ltd., Shanghai, China, www.aladdin-e.com). Tris-(hydroxymethyl)aminomethane (Tris), 4-(2-hydroxyethyl) piperazine-1-ethanesulfonic acid (HEPES), RNase inhibitor, diethypyrocarbonate (DEPC), and DNA and microRNA sequences were provided by Sangon (Sangon Biotech (Shanghai) Co. Ltd., Shanghai, China, www.sangon.com). The DNA and microRNA sequences were used as received. Their sequences are listed in Table 1. The total microRNA extractions from *A. thaliana* seedlings were kindly provided by Prof. Y. Han's lab at Hefei University of Technology. The DNA stock solution was prepared using Tris-HCl buffer (10 mM pH 7.4 Tris-HCl, 1.0 mM EDTA). The solutions used in all experiments were prepared using DEPC-treated water.

Instruments and measurement

The transmission electron microscopy (TEM) image was recorded by JEM-1400 flash (JEOL Ltd., Tokoyo, Japan, www.jeol.co.jp). X-ray photoelectron spectroscopy (XPS) measurements were performed on an ESCALAB250 X-ray photoelectron spectrometer (Thermo Fisher Scientific, CA, USA, www.thermofisher.com). Fourier transform infrared (FTIR) spectra were recorded with Nicolet 67 spectrometer (Thermo Fisher Scientific, CA, USA, www.thermofisher.com) in the range of 4000–500 cm^{-1}. Zeta analysis was measured with a Zetasizer Nano-ZS90 system (Malvern Instruments Ltd., Worcestershire, UK, www.malvernpanalytical.com). The UV-vis spectra were obtained on UV-4802 ultraviolet-visible spectrophotometer (Unico Shanghai Instrument Co., Ltd. Shanghai, China, www.unicosh.com.cn). Fluorescence measurements were performed using a F97pro fluorescence instrument (Shanghai Lengguang Tech. Co., Ltd., Shanghai, China, http://www.lengguang.com).

Table 1 DNA and microRNA sequences employed in the present work

Name	Sequences (from 5′ to 3′)
Target microRNA167	UGA AGC UGC CAG CAU GAU CUA
Probe DNA (pDNA)	TAG ATC ATG CTG GCA GCT TCA-$(CH_2)_6$-NH_2
Single-base mismatched microRNA (SM microRNA)	UGA AGC UGC ***G***AG CAU GAU CUA
Double-base mismatched microRNA (DM microRNA)	UGA ***C***GC UGC ***G***AG CAU GAU CUA
Three-base mismatched microRNA (TM microRNA)	UGA ***C***GC UGC ***G***AG CAU GA***C*** CUA
Non-complementary microRNA (NC microRNA)	CGG CUA CUG AGA CUG AUG UCA

Synthesis of Fe_3O_4@PDA nanoparticles

The Fe_3O_4@PDA core–shell nanoparticles were synthesized according to the reported method [30] with minor modification. Specifically, 50 mg of Fe_3O_4 NPs (~ 100 nM, Fig. S1 A) was dispersed in 50 mL Tris-HCl buffer (pH 8.5, 10 mM) containing 2 mg mL^{-1} of dopamine. The mixture was left reacting for 8 h at room temperature under stirring. The resultant product was separated and collected with a magnet. Subsequently, the obtained Fe_3O_4@ PDA NPs were washed with water several times, followed by drying at 40 °C under nitrogen atmosphere. Finally, the Fe_3O_4@PDA nanoparticles were dispersed in 10 mM HEPES buffer (pH 7.8, 2 mM Ca^{2+}) to a desired concentration and kept at 4 °C in refrigerator. The TEM image of Fe_3O_4@PDA nanoparticles shows that Fe_3O_4 nanoparticles are wrapped within thin films of PDA (Fig. S1 B), indicating successful preparation of Fe_3O_4@PDA nanoparticles. The prepared Fe_3O_4@PDA NPs also possess good magnetic property. This shows that there is no obvious negative effect of PDA on Fe_3O_4 magnetic property.

Preparation of CDs-labeled probe DNA

The synthesis of CDs was according to the method that described in the literature [31] with some modifications. Briefly, 2.5 g of citric acid and 1.5 mL of ethylenediamine were dissolved in 30 mL of water. Then, the mixture was transferred into a Teflon-lined autoclave and heated at 200 °C for 5 h. When the reaction was over, the reactor was naturally cool down to room temperature, and the obtained product of CDs was purified by dialyzing (12 times in 24 h) in a dialysis bag (retained molecular weight of 1 kDa).

The fluorescence tags of CDs-labeled probe DNA (CDs-pDNA) were prepared using well-established carbodiimide method. The –COOH groups in CDs were activated by mixing the CDs (2 mL) with a mixture (2 mL) of EDC (20 mg m L^{-1}) and NHS (10 mg mL^{-1}) in 10 mM HEPES buffer (pH 7.8), followed with sonication for 5 min. The mixture was then kept incubating for 1 h at 37 °C. After the addition of 50 μL of 100 μM pDNA, the mixture was incubated for another 1 h at 37 °C. The obtained CDs-pDNA were stored in the refrigerator at 4 °C for future use. Agarose gel electrophoresis analysis for CDs-pDNA was conducted (Fig. S2) and the details are described in ESM.

Determination of microRNA-167

For determination of microRNA-167, 50 μL of Fe_3O_4@PDA suspension (2 mg mL^{-1} in pH 7.8 of 10 mM HEPES buffer contained 2 mM Ca^{2+}) was added into 200 μL of CDs-pDNA solution. The mixture was diluted to a final volume of 1.5 mL using HEPES buffer (pH 7.8, 10 mM, 2 mM Ca^{2+}) with 20 U RNase inhibitor. It was then incubated for 1 h to quench the fluorescence. Afterward, the free CDs and excessive pDNA were removed by magnetic separation. The CDs-pDNA-Fe_3O_4@PDA complex was gathered and redispersed after three washes. Subsequently, 20 μL of microRNA-167 with various concentrations was added into the mixture. The incubation lasted for 30 min at 37 °C with continuous shaking. Finally, the released CDs-pDNA-microRNA-167 complex was magnetically separated from unhybridized CDs-pDNA-Fe_3O_4@PDA. The recovered fluorescence spectra were measured on a fluorescence spectrometer. The emission intensity at 445 nm under the fixed excitation wavelength of 360 nm was recorded. The output signal was calculated according to the equation as follows:

$$\text{output signal} = \frac{(F - F_0)}{F_0}$$

where F and F_0 represent the fluorescence intensities of the proposed assay after magnetic separation with or without target microRNA-167, respectively.

Results and discussion

Characterization of CDs and CDs-pDNA

The shape and size of CDs were characterized by TEM. As can be seen from Fig. 1a, the spherical particles are distributed uniformly. The particle size of a majority CDs is 3.0 ± 0.3 nm, and the average diameter of 104 particles in Fig. 1a is about 2.8 ± 0.7 nm (Fig. 1b).

The optical features of the CDs were investigated by UV-vis absorption and fluorescence spectra (Fig. 1c). In UV-vis spectrum of CDs, a broad and strong absorbance at 357 nm corresponding to n–π* [32] is observed. The strong absorption that leads to strong emission is owing to the excited-state energy trapping by the surface state [33]. The optimal excitation (EX) and emission (EM) wavelength of CDs in the fluorescence spectra are at 360 and 445 nm, respectively. The color of the CDs is light brown with high transparency under daylight (Fig. 1c, inset: left). It changes into deep blue when exposed to ultra-violet light at 360 nm (Fig. 1c, inset: right).

The elemental components of CDs and CDs-pDNA were analyzed by XPS (Fig. 1d). The XPS patterns show the presence of C, N, and O elements in both CDs and CDs-pDNA. The percentage of N in CDs-pDNA is ~ 18.4%, which is higher than that in CDs of 14.7%. Another peak in CD-pDNA is observed at 197.08 eV, which is assigned to the binding energy of P2s [34]. The increased percentage of N and the presence of P element indicate the successful preparation of CDs-pDNA.

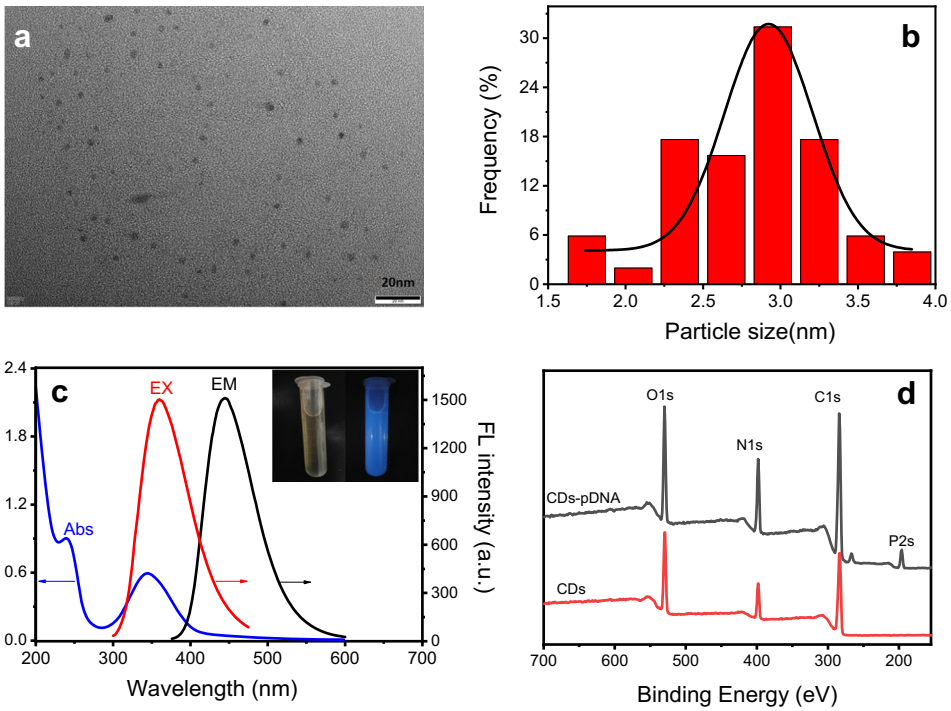

Fig. 1 **a** TEM image of CDs. **b** Particle size distribution of CDs. **c** UV–vis absorption (Abs), excitation (EX), and emission (EM) spectra of CDs in aqueous solutions. Inset shows photographs of CDs in aqueous solutions under room light (left) and under 360 nm UV lamp light (right). **d** XPS patterns of the prepared CDs and CDs-pDNA

Characterization of Fe_3O_4@PDA NPs

The FT-IR spectra of Fe_3O_4 NPs, PDA, and Fe_3O_4@PDA are shown in Fig. 2a. In the spectrum of Fe_3O_4 NPs, the characteristic absorption peak at about 586 cm^{-1} relates to the Fe–O stretching vibration [35]. Four characteristic peaks at 1608, 1508, 1445, and 1274 cm^{-1} can be observed in the spectrum of PDA. The peaks located at 1608, 1508, and 1445 cm^{-1} can attribute to the vibration of C=C in the benzene ring of PDA [30, 36], and the peak at 1274 cm^{-1} to the stretching vibration of C–O in phenolic groups [36]. These typical absorption peaks in Fe_3O_4 NPs and PDA are also found in the spectrum of Fe_3O_4@PDA NPs. This indicates the successful coating of PDA on the surface of Fe_3O_4 NPs.

The successful preparation of Fe_3O_4@PDA was further proved by using zeta potential measurement. As can be seen from the results displayed in Fig. 2b, the zeta potential of Fe_3O_4 NPs is measured to be −31.9 mV. The zeta potential of Fe_3O_4@PDA in aqueous solution is −49.2 mV, which is much more negative than that of Fe_3O_4 NPs. Because PDA is an ampholyte polymer containing amine and phenolic hydroxyl groups, it is negatively charged in neutral/basic condition [37]. This leads to the decrease of zeta potential of Fe_3O_4@PDA. Such decrease also indicates the successful preparation of the core-shell nanostructure of Fe_3O_4@PDA. The zeta potential of Fe_3O_4@PDA NPs increased from −49.2 to −31.2 mV after incubating with Ca^{2+}, and subsequently decreased again to a value of −35.0 mV after incubating with pDNA. These changes demonstrate the attachment of pDNA onto Fe_3O_4@PDA with the assistance of Ca^{2+}.

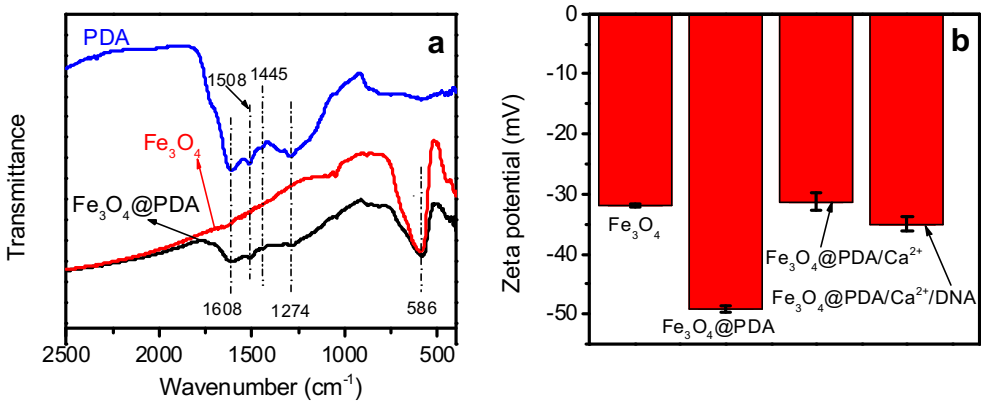

Fig. 2 **a** FT-IR spectra of Fe_3O_4 NPs, PDA, and Fe_3O_4@PDA NPs. **b** Zeta potential of Fe_3O_4 NPs, Fe_3O_4@PDA NPs, Fe_3O_4@PDA/Ca^{2+}, and Fe_3O_4@PDA/Ca^{2+}/pDNA

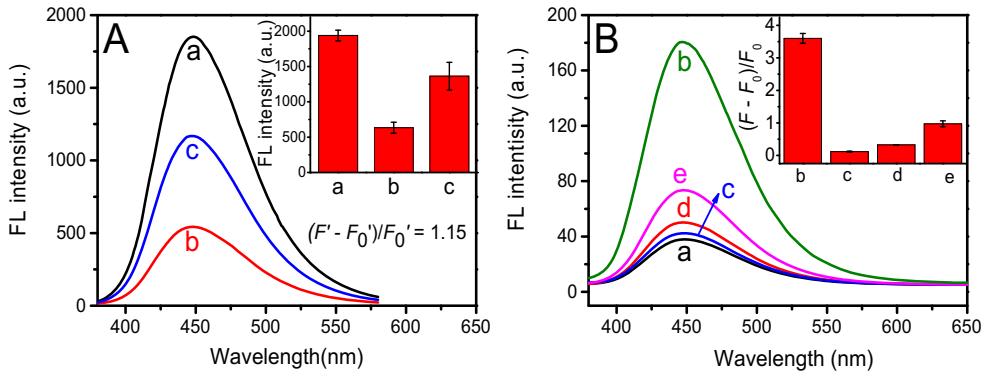

Fig. 3 **A** The fluorescence recovery ability of CDs without magnetic separation. (*a*) CDs-pDNA, (*b*) CDs-pDNA/Fe_3O_4@PDA, and (*c*) microRNA-167/CDs-pDNA/Fe_3O_4@PDA. Condition: the concentrations of Ca^{2+} and microRNA-167 were 2 mM and 50 nM, respectively. Inset: the column diagram of fluorescence intensity corresponding to the curves. **B** Fluorescence intensity of CDs-pDNA under various conditions: (*a*) quenched with Fe_3O_4@PDA NPs, (*b*) recovered with 50 nM microRNA-167 in presence of 2 mM Ca^{2+}, (*c*) quenched with Fe_3O_4@PDA NPs then recovered without adding microRNA-167 in presence of 2 mM Ca^{2+}, (*d*) quenched with Fe_3O_4 NPs and then recovered with 50 nM microRNA-167 in presence of 2 mM Ca^{2+}, and (*e*) quenched with Fe_3O_4@PDA NPs and then recovered with 50 nM microRNA-167 in absence of 2 mM Ca^{2+}. Inset: relative fluorescence intensities $(F - F_0)/F_0$ under various conditions. The fluorescence intensity was measured after magnetic separation

The feasibility of biosensing method

The principle of the biosensing method for microRNA-167 is based on Ca^{2+}-assisted FRET. The fluorescence stability of CDs in Ca^{2+}-contained aqueous solution was evaluated first, and the results are shown in Fig. S3. It is obvious that Ca^{2+} barely show unwelcomed influence on the fluorescence intensity of CDs. This indicates good fluorescence stability of CDs in Ca^{2+}-contained aqueous solution. The sensing strategy is well described in Fig. 3 by fluorescent measurement. Figure 3A explains the quenching ability of Fe_3O_4@PDA and the recovered intensity of CDs without magnetic separation. In presence of Ca^{2+}, the initial fluorescence intensity of CDs-pDNA is about 1938 (curve a). It decreases dramatically to 634 (F_0', curve b) after quench with Fe_3O_4@PDA NPs. The fluorescence intensity of CDs-pDNA is quenched ~ 67.3% by Fe_3O_4@PDA NPs compared with the initial intensity of CDs-pDNA. This shows good quenching ability of Fe_3O_4@PDA NPs. The intensity afterward increases to 1363 (F', curve c) after incubating with 50 nM of target microRNA-167. In presence of the target microRNA-167, pDNA can hybridize with microRNA-167 to form double chains of CDs-pDNA-microRNA-167. Because of stronger affinity between pDNA and target microRNA-167, the hybridization event can break π stacking interaction between pDNA and Fe_3O_4@PDA NPs. As a result, the hybridized complex of CDs-pDNA-microRNA-167 will release from the surface Fe_3O_4@PDA NPs and transfer into solution. This is the reason for the recovery of CDs intensity at 445 nm. The florescence intensity recovers back to ~ 70.3% of the initial intensity of CDs-pDNA, demonstrating an excellent intensity recovery of CDs.

The intensities of CDs under various conditions were measured (Fig. 3B) and the relative fluorescence intensities [$(F - F_0)/F_0$] (Fig. 3B, inset) were calculated. The merit of the biosensing platform with twice magnetic separations can be explained by Fig. 3B. The fluorescence intensity (F_0, Fig. 3B, curve a) of CDs decreases sharply (compared with curve b in Fig. 3A) after separating and removing free CDs from CDs-pDNA/Fe_3O_4@PDA. After incubating CDs-pDNA/Fe_3O_4@PDA in solution containing 50 nM microRNA-167

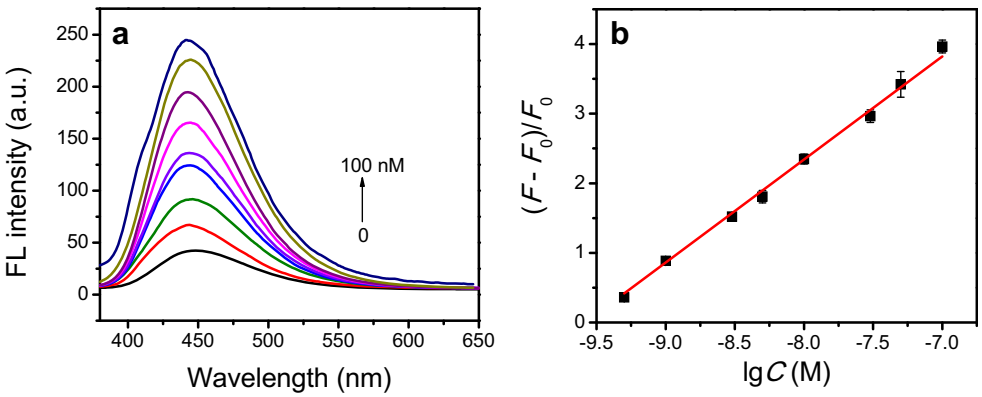

Fig. 4 **a** Fluorescence response of the proposed assay with magnetic separation in the presence of target microRNA-167 with increasing concentration (from bottom to up: 0, 0.5, 1, 3, 5, 10, 30, 50, 100 nM). **b** The relationship between $(F - F_0/F_0)$ and common logarithm of target microRNA-167 concentration

Table 2 FRET biosensors for DNA/microRNA detection

Strategy	Target	Detection time	Linear range (nM)	Detection limit (pM)	Ref.
FRET from FAM to PDA nanospheres mediated by metal coordination	DNA (24 bases)	Less than 2 h	0–50	400	[22]
FRET from MoS_2 QDs to FAM PDA	microRNA-21	In 1 h	5–150	380 in aqueous solution 520 in artificial cerebrospinal fluid	[25]
FRET from AuNCs to PDA nanospheres with DNase-I-assisted target recycling amplification	microRNA-21 Let-7a	Less than 2 h	0.01–2.0 0.01–2.5	4.2 3.6	[26]
MnO_2 nanosheet-mediated ratiometric fluorescence biosensor using catalyzed hairpin assembly (CHA) signal amplification	microRNA-21	In 1 h	0.1–20	73	[38]
FRET from CDs to Black hole quencher 1	microRNA-21	In 1 h	5–160	300	[39]
FRET from CDs to Fe_3O_4@PDA in presence of Ca^{2+}	microRNA-167	Less than 2 h	0.5–100	76	This work

and 2 mM Ca^{2+}, the second magnetic separation was performed. It can separate Fe_3O_4@PDA from CDs-pDNA and microRNA complex (hybridization complex). The corresponding intensity of CDs increases and recovers notably (Fig. 3B, curve b). The calculated $(F - F_0)/F_0$ is about 3.49, which is much more higher than $(F' - F_0')/F_0'$ (1.15, without magnetic separation). This indicates the twice-magnetic separation improves the sensitivity of the biosensing method. The improved intensity from magnetic separation is resulted from relatively low F_0 and high F. The decreased background signal is due to the first magnetic separation. The increased recovery intensity is because of eliminating the absorption and scattering effects from Fe_3O_4@PDA using the second magnetic separation. Moreover, it is clear that with the assistance of Ca^{2+}, the value of $(F - F_0)/F_0$ is the largest among those values without recovery of target microRNA, quenched with Fe_3O_4 NPs, and without assistance of Ca^{2+} (Fig. 3B, inset). This result demonstrates further sensitivity improvement of the biosensing system from Ca^{2+}. The good quenching ability of Fe_3O_4@PDA NPs, the excellent recovered intensity of CDs, and the assistance of Ca^{2+} prove the feasibility of our biosensing method.

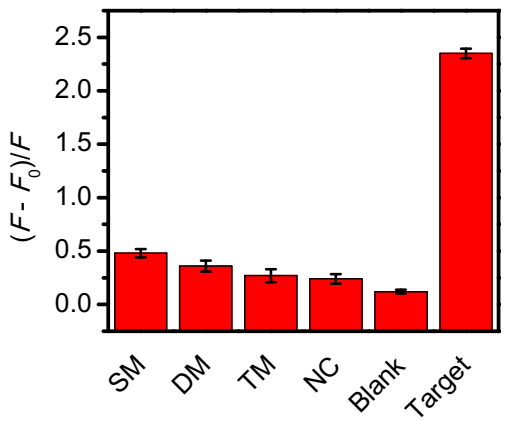

Fig. 5 The selectivity of the biosensor

Analytical performance of the biosensor

The following parameters of microRNA-167 biosensor were optimized: (a) concentration of Fe_3O_4@PDA, (b) concentration of Ca^{2+}, (c) pH value of hybridization buffer, (d) concentration of pDNA, (e) hybridization time, and (f) hybridization temperature. The data are given in Fig. S4. It is clear that the following experimental conditions give the best results: (a) Fe_3O_4@PDA concentration of 2 mg mL^{-1}, (b) Ca^{2+} concentration of 2 mM, (c) pH value of 7.8, (d) pDNA concentration of 120 nM, (e) hybridization time of 30 min, and (f) hybridization temperature of 37 °C.

The biosensor for microRNA-167 determination was conducted under optimized conditions. The fluorescence intensities of CDs recovered by various concentrations of target microRNA-167 are shown in Fig. 4a. With increasing amount of target microRNA-167, the fluorescence intensity of CDs enhances as expected due to the increasing released complex of CDs-pDNA-microRNA-167. The relative fluorescence intensity $(F - F_0)/F_0$ shows good linear relationship to the common logarithm of the target microRNA-167 concentration in range of 0.5–100 nM. Such relationship is written as a linear equation of $(F - F_0)/F_0 = 1.48\lg C$ (M) + 14.20, R = 0.997 (Fig. 4b). The limit of detection is calculated to be 76 pM ($S/N = 3$). The biosensing can be finished in less than 2 h. The analytical performances regarding detection time, linear range, and detection limit of the microRNA-167 biosensor and other FRET-based microRNA [25, 26, 38, 39] or DNA [22] biosensors are listed Table 2. As can be noticed from the table, our biosensor also shows good analytical performance in detecting microRNA.

The selectivity and specificity of the biosensor towards microRNA-167 over other microRNA sequences were investigated. These measurements were conducted under optimal conditions, and the concentrations of these mismatched sequences including SM microRNA-167, DM microRNA-167,

TM microRNA-167, and NC microRNA were 100 nM (10× higher than the target microRNA). The calculated $(F - F_0)/F_0$ values related to the mismatched sequences are much more lower than that related to target microRNA (Fig. 5). The fluorescence intensities recovered by mismatched microRNA-167 sequences is slightly increased compared with the blank signal. The results suggest that only target microRNA-167 can trigger the signal recovery strategy perfectly. These results show that the biosensor has good selectivity towards microRNA-167.

The method was applied to determination of microRNA-167 in total microRNA extractions from *A. thaliana* seedlings. The results are listed in Table S1. The method was validated by standard addition method. The recoveries are 96.4% and 98.3% (n = 6), respectively, and with the relative standard deviation (RSD) of 7.0% and 5.9%. This indicates good detection accuracy of our detecting method.

Conclusions

In conclusion, we successfully developed a rapid, sensitive, and selective FRET-based biosensor for determination of microRNA-167 using CDs as donor and Fe_3O_4@PDA NPs as acceptor. The recovered fluorescence intensity by target microRNA-167 is because of different affinity of Fe_3O_4@PDA NPs to ssDNA sequences and hybridized complex. The good sensitivity of the biosensor is achieved through (1) lowering the background signal by application of twice-magnetic separation, (2) excellent quenching ability of Fe_3O_4@PDA NPs, and (3) strong adsorbing ability of Fe_3O_4@PDA NPs enhanced by Ca^{2+}. The biosensor possesses good selectivity, sensitivity, and reliability that can be used in determination of microRNA-167 in microRNA extractions from *A. thaliana* seedlings. We anticipate a deep-going application of this method, making clear the relationship between the expression level of microRNA-167 and the treated amount of phytohormone IAA in model plants.

Funding information The project is supported by the National Natural Science Foundation of China (Grant No. 31772099, 31401573 and 21505071), the China Postdoctoral Science Foundation (Grant No. 2017 T100446, 2016M592050), the Natural Science Foundation of Anhui Province (No. 1908085MC98), the Anhui Key Research and Development Program (No. 201904a06020030), and the Fundamental Research Funds for the Central Universities (No. JZ2018HGTB0245).

Compliance with ethical standards

Conflict of interest The authors declare that they have no competing interests.

References

1. Curaba J, Singh MB, Bhalla PL (2014) MiRNAs in the crosstalk between phytohormone signalling pathways. J Exp Bot 65:1425–1438
2. Arora S, Pandey DK, Chaudhary B (2019) Target-mimicry based diminution of miRNA167 reinforced flowering-time phenotypes in tobacco via spatial-transcriptional biases of flowering-associated miRNAs. Gene 682:67–80
3. Yao X, Chen J, Zhou J, Yu H, Ge C, Zhang M, Gao X, Dai X, Yang ZN, Zhao Y (2019) An essential role for mirna167 in maternal control of embryonic and seed development. Plant Physiol 180: 453–464
4. Kinoshita N, Wang H, Kasahara H, Liu J, MacPherson C, Machida Y, Kamiya Y, Hannah MA, Chuaa NH (2012) IAA-Ala Resistant3, an evolutionarily conserved target of microRNA-167, mediates Arabidopsis root architecture changes during high osmotic stress. Plant Cell 24:3590–3602
5. Srivastava S, Srivastava AK, Supraasanna P, D'Souza SF (2013) Identification and profiling of arsenic stress-induced microRNAs in *Brassica juncea*. J Exp Bot 64:303–315
6. Várallyay É, Burgyán J, Havelda Z (2008) MicroRNA detection by northern blotting using locked nucleic acid probes. Nat Protoc 3: 190–196
7. Zhi F, Chen X, Wang S, Xia X, Shi Y, Guan W, Shao N, Qu H, Yang C, Zhang Y, Wang Q, Wang R, Zen K, Zhang CY, Zhang J, Yang Y (2010) The use of hsa-miR-21, hsa-miR-181b and hsa-miR-106a as prognostic indicators of astrocytoma. Eur J Cancer 46:1640–1649
8. Konishi H, Ichikawa D, Komatsu S, Shiozaki A, Tsujiura M, Takeshita H, Morimura R, Nagata H, Arita T, Kawaguchi T, Hirashima S, Fujiwara H, Okamoto K, Otsuji E (2012) Detection of gastric cancer-associated microRNAs on microRNA microarray comparing pre- and post-operative plasma. Br J Cancer 106:740–747
9. Kilic T, Erdem A, Ozsoz M, Carrara S (2018) microRNA biosensors: opportunities and challenges among conventional and commercially available techniques. Biosens Bioelectron 99:525–546
10. Dong H, Lei J, Ding L, Wen Y, Ju H, Zhang X (2013) MicroRNA: function, detection, and bioanalysis. Chem Rev 113:6207–6233
11. Xiao Q, Li J, Jin X, Liu Y, Huang S (2019) Ultrasensitive electrochemical microRNA-21 biosensor coupling with carboxylate-reduced graphene oxide-based signal-enhancing and duplex-specific nuclease-assisted target recycling. Sensors Actuators B Chem 297:126740
12. Wu Y, He Y, Yang X, Yuan R, Chai Y (2018) A novel recyclable surface-enhanced Raman spectroscopy platform with duplex-specific nuclease signal amplification for ultrasensitive analysis of microRNA 155. Sensors Actuators B Chem 275:260–266
13. Li X, Wang T, Luo Y, Asiri AM, Chen S, Sun X (2020) Biomimetic assembly of a polydopamine layer on graphene as an electron gate for fluorescent microRNA detection in living cells. ChemBioChem. https://doi.org/10.1002/cbic.201900548
14. Li M, Xu X, Cai QY, Luo XJ, Zhou ZG, Xu GH, Xie YR (2019) Graphene oxide-based fluorometric determination of microRNA-141 using rolling circle amplification and exonuclease III-aided recycling amplification. Microchim Acta 186:531
15. Wu H, Wu J, Liu Y, Wang H, Zou (2019) Fluorometric determination of microRNA using arched probe-mediated isothermal exponential amplification combined with DNA-templated silver nanoclusters. Microchim Acta 186:715
16. Oh HJ, Kim J, Park H, Chung S, Hwang DW, Lee DS (2019) Graphene-oxide quenching-based molecular beacon imaging of exosome-mediated transfer of neurogenic miR-193a on microfluidic platform. Biosens Bioelectron 126:647–656

17. Liu Y, Jiang L, Fan X, Liu P, Xu S, Luo X (2019) Intracellular fluorometric determination of microRNA-21 by using a switch-on nanoprobe composed of carbon nanotubes and gold nanoclusters. Microchim Acta 186:447
18. Miao X, Cheng Z, Ma H, Li Z, Xue N, Wang P (2018) Label-free platform for microRNA detection based on the fluorescence quenching of positively charged gold nanoparticles to silver nanoclusters. Anal Chem 90:1098–1103
19. Oudeng G, Au M, Shi J, Wen C, Yang M (2018) One-step in situ detection of miRNA-21 expression in single cancer cells based on biofunctionalized MoS_2 nanosheets. ACS Appl Mater Interfaces 10:350–360
20. Xi Q, Zhou DM, Kan YY, Ge J, Wu ZK, Yu RQ, Jiang JH (2014) Highly sensitive and selective strategy for microRNA detection based on WS_2 nanosheet mediated fluorescence quenching and duplex-specific nuclease signal amplification. Anal Chem 86: 1361–1365
21. Qiang W, Li W, Li X, Chen X, Xu D (2014) Bioinspired polydopamine nanospheres: a superquencher for fluorescence sensing of biomolecules. Chem Sci 5:3018–3024
22. Meng Y, Liu P, Zhou W, Ding J, Liu J (2018) Bioorthogonal DNA adsorption on polydopamine nanoparticles mediated by metal coordination for highly robust sensing in serum and living cells. ACS Nano 12 (2018) 9070–9080
23. Zhu S, Zhang J, Qiao C, Tang S, Li Y, Yuan W, Li B, Tian L, Liu F, Hu R, Gao H, Wei H, Zhang H, Sun H, Yang B (2011) Strongly green-photoluminescent graphene quantum dots for bioimaging applications. Chem Commun 47:6858–6860
24. Hamd-Ghadareh S, Hamah-Ameen BA, Salimi A, Fathi F, Soleimani F (2019) Ratiometric enhanced fluorometric determination and imaging of intracellular microRNA-155 by using carbon dots, gold nanoparticles and rhodamine B for signal amplification. Microchim Acta 186:469
25. Yu X, Hu L, Zhang F, Wang M, Xia Z, Wei W (2018) MoS_2 quantum dots modified with a labeled molecular beacon as a ratiometric fluorescent gene probe for FRET based detection and imaging of microRNA. Microchim Acta 185:239
26. Xu S, Nie Y, Jiang L, Wang J, Xu G, Wang W, Luo X (2018) Polydopamine nanosphere/gold nanocluster (Au NC)-based nanoplatform for dual color simultaneous detection of multiple tumor-related microRNAs with DNase-I-assisted target recycling amplification. Anal Chem 90:4039–4045
27. Jiang Y, Ma X, Shao X, Wang M, Jiang Y, Miao P (2019) Chameleon silver nanoclusters for ratiometric sensing of miRNA. Sensors Actuators B Chem 297:126788
28. Ye Y, Mao S, He S, Xu X, Cao X, Wei Z, Gunasekaran S (2020) Ultrasensitive electrochemical genosensor for detection of CaMV 35S gene with Fe_3O_4-Au@Ag nanoprobe. Talanta 206:120205
29. Shen X-P, Ge J, Chen J, She Y-M, Meng H-M, Li Z-H, Qu L-B (2019) A novel fluorescence method for the highly sensitive detection of T4 polynucleotide kinase based on polydopamine nanotubes. New J Chem 43:16753–16758
30. Li N, Hao X, Kang BH, Xu Z, Shi Y, Li NB, Luo HQ (2016) Enzyme-free fluorescent biosensor for the detection of DNA based on core-shell Fe_3O_4 polydopamine nanoparticles and hybridization chain reaction amplification. Biosens Bioelectron 77:525–529
31. Zhu S, Meng Q, Wang L, Zhang J, Song Y, Jin H, Zhang K, Sun H, Wang H, Yang B (2013) Highly photoluminescent carbon dots for multicolor patterning, sensors, and bioimaging. Angew Chem Int Ed 52:3953–3957
32. Dela Cruz MIS, Thongsai N, de Luna MDG, In I, Paoprasert P (2019) Preparation of highly photoluminescent carbon dots from polyurethane: optimization using response surface methodology and selective detection of silver (I) ion. Colloids Surf A 568:184–194
33. Li H, He X, Kang Z, Huang H, Liu Y, Liu J, Lian S, Tsang CHA, Yang X, Lee S-T (2010) Water-soluble fluorescent carbon quantum dots and photocatalyst design. Angew Chem Int Ed 26:4532–4536
34. Zhu W, Shen X, Zhu C, Li B, Hong J, Zhou X (2018) Turn-on fluorescent assay based on purification system via magnetic separation for highly sensitive probing of adenosine. Sensors Actuators B Chem 259:855–861
35. Yavuz E, Tokalıoğlu Ş, Patat Ş (2018) Core–shell Fe_3O_4 polydopamine nanoparticles as sorbent for magnetic dispersive solid-phase extraction of copper from food samples. Food Chem 263:232–239
36. Gao X, Yao X, Zhong Z, Jia L (2018) Rapid and sensitive detection of Staphylococcus aureus assisted by polydopamine modified magnetic nanoparticles. Talanta 186:147–153
37. Wang Y, Ma X, Ding C, Jia L (2015) PH-responsive deoxyribonucleic acid capture/release by polydopamine functionalized magnetic nanoparticles. Anal Chim Acta 862:33–40
38. Wang S, Wang L, Xu X, Li X, Jiang W (2019) MnO_2 nanosheet-mediated ratiometric fluorescence biosensor for microRNA detection and imaging in living cells. Anal Chim Acta 1063:152–158
39. Mahani M, Mousapour Z, Divsar F, Nomani A, Ju H (2019) A carbon dot and molecular beacon based fluorometric sensor for the cancer marker microRNA-21. Microchim Acta 186:132